 CMC, vol.5, no.3, pp.161-172, 2007

A Micromechanical Approach to Simulate Rubberlike Materials with Damage

M. Timmel[1], M. Kaliske[1], S. Kolling[2] and R. Mueller[3]

Abstract: A damage approach based on a material model with microstructural evolution is presented. In contrast to phenomenological constitutive laws, the material response is given by mechanisms at the microscale. At first, a micromechanical substructure is chosen, which represents the overall material behaviour. Then the system is described using a micromechanical model. A geometrical modification of the microstructure is allowed to minimize the total energy. Consequently, the global stiffness is reduced. In this context, thermodynamical considerations are based on configurational forces. With the help of the discussed approach, void growth phenomena of materials, which lead to softening behaviour, can be taken into account numerically. In this article, the influence of the microstructure in hyperelastic materials is investigated. Hereby, we discuss evolution methods for small and finite strain problems. Finally, the implementation of this damage approach in an explicit finite element solver is described in detail.

Keyword: Configurational Forces, Micromechanics, Damage, Finite Strains, Hyperelasticity.

1 Introduction

In the case of cyclic loading, softening effects are observed experimentally and have to be taken into account in the continuum description of the material. This softening behaviour is based on the initiation and on the evolution of microcracks and microvoids. To include softening effects in numerical calculations, phenomenological models are widely used, see Lemaitre and Desmorat (2005). That way, damage behaviour is described by modifying the constitutive elastic formulation with an additional internal variable d. This quantity describes the decrease of the structural potential energy in dependence of the loading history:

$$\Psi = \Psi(\underline{\mathbf{C}}, \mathrm{d}) = (1-\mathrm{d})\Psi_0(\underline{\mathbf{C}}) \quad (0 \leq \mathrm{d} \leq 1). \quad (1)$$

For finite strains, a potential Ψ is given in terms of the Right Cauchy Green strain $\underline{\mathbf{C}}$ as shown in Equation (1). Inserting (1) into the Clausius Duhem inequality yields finally the reduced dissipation inequality

$$\mathscr{D} = -\Psi_0(\underline{\mathbf{C}})\,\dot{\mathrm{d}} \leq 0, \quad (2)$$

see Coleman and Noll (1963). This leads to a relation $\underline{\tilde{\boldsymbol{\sigma}}} = (1-\mathrm{d})\underline{\boldsymbol{\sigma}}$ that maps $\underline{\tilde{\boldsymbol{\sigma}}}$ of the damaged formulation to $\underline{\boldsymbol{\sigma}}$ of the undamaged material response based on a hyperelastic potential Ψ_0. The damage measure d is related to the volume fraction of microvoids with respect to a representative volume.

Since stress-strain relations depend on the loading process, a functional correlation $\dot{\mathrm{d}} = f(\Psi_0(\underline{\mathbf{C}}))$ is defined based on the dissipation inequality. In this context, a detailed description of the application of phenomenological approaches in hyperelastodynamics is given in Timmel, Kaliske and Kolling (2004).

Damage approaches based on internal variables are restricted to non-complex material behaviour. An improved approximation can be obtained by the description on the microscale. In Mueller (2001) and Kolling (2001), the change of the stiffness in metals is modeled by diffusive or martensic phase transitions.

Based on such a formulation, softening can be approximated by the behaviour of soft inclusions,

[1] Institute for Structural Mechanics, University of Leipzig, Germany.
[2] DaimlerChryslerAG, Sindelfingen, Germany.
[3] Institute of Mechanics, TU Darmstadt, Germany.

which are embedded in a stiffer matrix material. During the loading process, the configuration of these inclusions is modified by work conjugated driving forces. For the suggested damage model, a microsystem is defined representing the overall material behaviour. The global response of the material is obtained by homogenization.

This method is implemented into an explicit finite element program. With the help of this numerical solver, the response of the material can also be analyzed in impact simulations.

2 Two Scale Approach

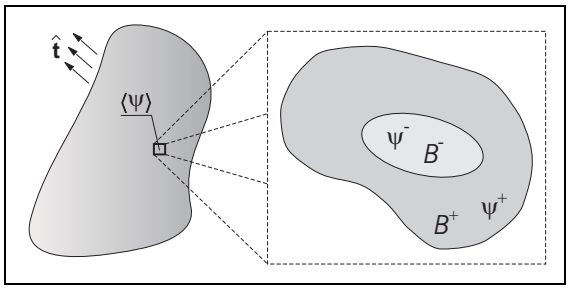

Figure 1: micro-macroscale-interaction

Based on Figure 1, the principle of our two scale damage model can be illustrated. We define a homogeneous global structure which is subjected to an arbitrary external loading $\hat{\mathbf{t}}$. The microscopic detail of this structure is characterized by a heterogeneous constitution, whereby B^+ denotes a volume consisting of a stiffer material with a hyperelastic strain energy density Ψ^+. Additionally, a second phase with the volume B^- and the potential Ψ^- is included in the microscale model to represent a material defect. At the macroscale, this heterogeneous material distribution is modeled by a macroscopic (homogenized) strain energy $\langle\Psi\rangle$. During loading process, the microstructure is able to change its configuration. To minimize the total energy in case of material softening, the expansion of the domain B^- is the logical consequence for the structural behaviour. In the following, a model for the description of the evolution of these embedded soft inclusions will be presented. Thereby, the inclusions are geometrically approximated by ellipsoids. This restriction is justified due to frequently appearances of voids in reality. Moreover, numerical investigations can be carried out with an improved efficiency.

2.1 Micromechanical Formulation

Taking microstructural evolution into account, some basic principles are discussed. Based on Figure 2, we define a general hyperelastic two phase system in its reference configuration.

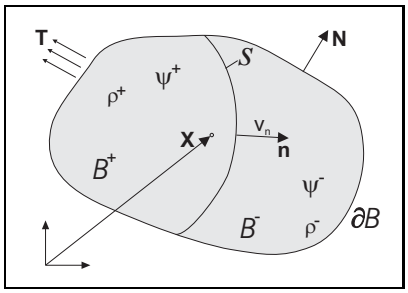

Figure 2: micromechanical model

The phases are separated by a sharp phase boundary S. The vector $\mathbf{n}$ denotes the unit normal vector on S and the unit normal on the outer boundary ∂B is introduced with $\mathbf{N}$. The densities of phases are assumed to be identical ($\rho^- = \rho^+ = \rho$). The loading of the microstructure is given by a surface traction $\underline{\mathbf{T}} = \underline{\mathbf{P}}\mathbf{N}$, where $\underline{\mathbf{P}}$ is the First Piola-Kirchhoff stress, or a boundary displacement $\mathbf{x} = \underline{\mathbf{F}}\mathbf{X}$, where $\underline{\mathbf{F}}$ is the deformation gradient. The local free energy

$$\Psi(\underline{\mathbf{F}}, \mathbf{X}) = \begin{cases} \Psi^-(\mathbf{X}) & \forall\, \mathbf{X} \in B^- \\ \Psi^+(\mathbf{X}) & \forall\, \mathbf{X} \in B^+ \end{cases} \tag{3}$$

depends on the material position $\mathbf{X}$ explicitly.

An important point to describe the movement of the phase boundary S with the velocity v_n in normal direction is the formulation of the dissipation inequality. For this purpose, the local thermomechanical balance laws are used. Based on Schmidt (1997) and literature cited therein, thermomechanical formulations for the phase boundary S are given. In the following, body forces $\mathbf{f}$ are neglected and $[\![\,\cdot\,]\!] = (\cdot)^+ - (\cdot)^-$ denotes the jump of a quantity across the phase boundary.

At first, the momentum balance is given by

$$\begin{aligned} &\mathrm{Div}\underline{\mathbf{P}} + \rho\ddot{\mathbf{x}} = \mathbf{0} && \text{in } B^-/B^+ \\ &[\![\underline{\mathbf{P}}\mathbf{n}]\!] + \rho[\![\dot{\mathbf{x}}]\!]\mathrm{v_n} = \mathbf{0} && \text{on } S \end{aligned} . \tag{4}$$

The rotational momentum balance yields the symmetry

$$\underline{\mathbf{P}}\,\underline{\mathbf{F}}^{\mathrm{T}} = \underline{\mathbf{F}}\,\underline{\mathbf{P}}^{\mathrm{T}}, \tag{5}$$

where no additional condition on the phase boundary is pointed out.

The energy balance can be given by

$$\begin{aligned} &\rho\dot{\mathrm{u}} - \underline{\mathbf{P}} : \dot{\underline{\mathbf{F}}} = 0 && \text{in } B^-/B^+ \\ &\rho[\![\mathrm{u} + \frac{1}{2}|\dot{\mathbf{x}}|^2]\!]\mathrm{v_n} + [\![(\underline{\mathbf{P}}\mathbf{n})\cdot\dot{\mathbf{x}}]\!] = 0 && \text{on } S \end{aligned} , \tag{6}$$

where u denotes the specific internal energy.

Finally, the entropy balance of the two phase system is stated by

$$\begin{aligned} &\rho\dot{\eta}\Theta - \omega_{\mathrm{B}}\Theta = 0 && \text{in } B^-/B^+ \\ &\rho\Theta[\![\eta]\!]\mathrm{v_n} - \omega_{\mathrm{S}}\Theta = 0 && \text{on } S \end{aligned} . \tag{7}$$

Here, η is the entropy density and Θ denotes the absolute temperature. ω_B and ω_S describe the production of entropy in volume and on the phase boundary, respectively.

Due to the restriction of identic densities ($\rho^+ = \rho^-$), the mass balance is presumed.

In accordance with the second law of thermodynamics ($\omega_B \geq 0,\ \omega_S \geq 0$) and defining the free energy $\Psi = \rho(\mathrm{u} - \eta\Theta)$, Equations $(6)_1$ and $(7)_1$ result in the dissipation inequality in the bulk:

$$\underline{\mathbf{P}} : \dot{\underline{\mathbf{F}}} - \dot{\Psi} = \omega_B\Theta \geq 0. \tag{8}$$

With Equations $(6)_2$ and $(7)_2$, we obtain in the same way the dissipation inequality

$$[\![\Psi + \frac{1}{2}\rho|\dot{\mathbf{x}}|^2]\!]\mathrm{v_n} + [\![(\underline{\mathbf{P}}\mathbf{n})\cdot\dot{\mathbf{x}}]\!] = \omega_{\mathrm{S}}\Theta \geq 0 \tag{9}$$

on the phase interface. The first part of Equation (9) corresponds to the total energy as the sum of free energy and kinetic energy. Henceforth, the middle term of (9) shall be reformulated, see Mueller (2001). In this context, we use the compatibility $[\![\dot{\mathbf{x}}]\!] = -\mathrm{v_n}[\![\underline{\mathbf{F}}]\!]\mathbf{n}$, the momentum balance (Equation (4)), and the identity $[\![ab]\!] = [\![a]\!]\langle\!\langle b\rangle\!\rangle + \langle\!\langle a\rangle\!\rangle[\![b]\!]$, where $\langle\!\langle\cdot\rangle\!\rangle = \frac{1}{2}[(\cdot)^+ + (\cdot)^-]$. At first, the middle term is modified by

$$\begin{aligned} [\![(\underline{\mathbf{P}}\mathbf{n})\cdot\dot{\mathbf{x}}]\!] = &-\rho\mathrm{v_n}[\![\dot{\mathbf{x}}]\!]\langle\!\langle\dot{\mathbf{x}}\rangle\!\rangle - \mathrm{v_n}[\![\underline{\mathbf{F}}\mathbf{n}]\!]\langle\!\langle\underline{\mathbf{P}}\mathbf{n}\rangle\!\rangle \\ &- \mathrm{v_n}\langle\!\langle\underline{\mathbf{F}}\mathbf{n}\rangle\!\rangle\cdot(\underbrace{[\![\underline{\mathbf{P}}\mathbf{n}]\!] + \rho[\![\dot{\mathbf{x}}]\!]\mathrm{v_n}}_{=\mathbf{0}}), \end{aligned} \tag{10a}$$

where the last part of Equation (10a) vanishes due to $(4)_2$. With

$$\begin{aligned} -\rho\mathrm{v_n^2}\langle\!\langle\underline{\mathbf{F}}\mathbf{n}\rangle\!\rangle[\![\dot{\mathbf{x}}]\!] = &-\rho\mathrm{v_n}[\![\dot{\mathbf{x}}]\!]\langle\!\langle\dot{\mathbf{x}}\rangle\!\rangle \\ &- \rho\mathrm{v_n^2}[\![\underline{\mathbf{F}}\mathbf{n}]\!]\langle\!\langle\dot{\mathbf{x}}\rangle\!\rangle - \rho\mathrm{v_n^2}[\![\underline{\mathbf{F}}\mathbf{n}]\!]\langle\!\langle\dot{\mathbf{x}}\rangle\!\rangle \end{aligned}$$

the reformulation of (10a) finally yields

$$\begin{aligned} [\![(\underline{\mathbf{P}}\mathbf{n})\cdot\dot{\mathbf{x}}]\!] = &-2\rho\mathrm{v_n}[\![\dot{\mathbf{x}}]\!]\langle\!\langle\dot{\mathbf{x}}\rangle\!\rangle \\ &- \mathrm{v_n}[\![\underline{\mathbf{F}}\mathbf{n}]\!]\langle\!\langle\underline{\mathbf{P}}\mathbf{n}\rangle\!\rangle - \mathrm{v_n}\langle\!\langle\underline{\mathbf{F}}\mathbf{n}\rangle\!\rangle[\![\underline{\mathbf{P}}\mathbf{n}]\!] \\ &- \rho\mathrm{v_n^2}[\![\underline{\mathbf{F}}\mathbf{n}]\!]\langle\!\langle\dot{\mathbf{x}}\rangle\!\rangle - \rho\mathrm{v_n^2}\langle\!\langle\underline{\mathbf{F}}\mathbf{n}\rangle\!\rangle[\![\dot{\mathbf{x}}]\!] \\ = &-\rho\mathrm{v_n}[\![|\dot{\mathbf{x}}|^2]\!] \\ &- \mathrm{v_n}[\![\underline{\mathbf{F}}^{\mathrm{T}}\underline{\mathbf{P}}]\!]\mathbf{n} \\ &- \rho\mathrm{v_n^2}[\![\underline{\mathbf{F}}^{\mathrm{T}}\dot{\mathbf{x}}]\!]\cdot\mathbf{n}\,. \end{aligned} \tag{10b}$$

Thus, the dissipation inequality on the phase boundary (9) can be written in the modified form

$$(\underbrace{\mathbf{n}\cdot[\![\underline{\mathbf{M}}]\!]\mathbf{n} - \mathrm{v_n}\rho\mathbf{n}\cdot[\![\underline{\mathbf{F}}^{\mathrm{T}}\dot{\mathbf{x}}]\!]}_{\tau_{\mathrm{n}}})\mathrm{v_n} = \omega_{\mathrm{S}}\Theta \geq 0. \tag{11}$$

In Equation (11), the quantity

$$\underline{\mathbf{M}} = \left(\Psi - \frac{1}{2}\rho|\dot{\mathbf{x}}|^2\right)\underline{\mathbf{1}} - \underline{\mathbf{F}}^{\mathrm{T}}\underline{\mathbf{P}} \tag{12}$$

denotes the dynamic energy momentum tensor according to Eshelby (1970). τ_{n} defines the driving force on S.

In the next step, we consider the Lagrangian $\mathscr{L}$ of the two phase system:

$$\mathscr{L} = T - \Psi = \frac{1}{2}\rho|\dot{\mathbf{x}}|^2 - \Psi(\underline{\mathbf{F}}, \mathbf{X}) \tag{13}$$

that is defined as the difference of the kinetic energy and the free energy. The change of the Lagrangian with respect to a translation of a material point can be investigated by computing the gradient

$$\begin{aligned} \nabla_{\mathbf{X}}\mathscr{L} &= \nabla_{\mathbf{X}}T - \nabla_{\mathbf{X}}\Psi \\ &= \rho(\nabla_{\mathbf{X}}\mathbf{v})^{\mathrm{T}}\mathbf{v} - \underline{\mathbf{P}} : \nabla_{\mathbf{X}}\underline{\mathbf{F}} - \left.\frac{\partial\Psi}{\partial\mathbf{X}}\right|_{\text{expl.}}. \end{aligned} \tag{14}$$

In Equation (14), the explicit derivative of the energy Ψ with respect to $\mathbf{X}$ yields a driving force. If we use the compatibility $\nabla_{\mathbf{X}}\dot{\mathbf{x}} = \dot{\underline{\mathbf{F}}}$, the local balance of momentum in volume according to Equation $(4)_2$, the identity $\underline{\mathbf{P}} : \nabla_{\mathbf{X}}\underline{\mathbf{F}} = \mathrm{Div}\left(\underline{\mathbf{F}}^{\mathrm{T}}\underline{\mathbf{P}}\right) - \underline{\mathbf{F}}^{\mathrm{T}}\,\mathrm{Div}\,\underline{\mathbf{P}}$ and $\nabla_{\mathbf{X}}\mathscr{L} = \mathrm{Div}\left(\mathscr{L}\,\underline{\mathbf{1}}\right)$, we achive the configurational force balance in the volume

$$\underbrace{\left(-\rho\left(\dot{\overline{\underline{\mathbf{F}}^{\mathrm{T}}\dot{\mathbf{x}}}}\right)\right)}_{:=-\dot{\mathbf{p}}} = \mathrm{Div}\underbrace{\left(-\mathscr{L}\,\underline{\mathbf{1}} - \underline{\mathbf{F}}^{\mathrm{T}}\underline{\mathbf{P}}\right)}_{\underline{\mathbf{M}}} + \underbrace{\left.\frac{\partial \Psi}{\partial \mathbf{X}}\right|_{\mathrm{expl.}}}_{\mathbf{g}_B} \tag{15}$$

(see Maugin (1993)), where we introduce the configurational force $\mathbf{g}_B$ and the pseudo momentum vector $\mathbf{p}$. To show that (15) is the bulk version of (11), we consider the generalized transport theorem

$$\begin{aligned}&\frac{d}{dt}\int_B \rho\Phi\,\mathrm{dV}\\ &\quad = \int_{\partial B}\Omega\cdot\mathbf{N}\,\mathrm{dA} + \int_{\mathrm{A}}\Pi_{\mathrm{S}}\,\mathrm{dA} + \int_{\mathrm{B}}\Pi_{\mathrm{V}}\,\mathrm{dV},\end{aligned} \tag{16}$$

where $A \subset S$ and its local form can be given by

$$\begin{aligned}&\rho\dot{\Phi} = \mathrm{Div}\Omega + \Pi_{\mathrm{V}} && \text{in } B^-/B^+\\ &-\rho[\![\Phi]\!]\mathrm{v_n} = [\![\Omega]\!]\mathbf{n} + \Pi_{\mathrm{S}} && \text{on } S\end{aligned}, \tag{17}$$

(see Schmidt (1997)). Based on Equations (15) and $(17)_1$ it can be seen that the general quantity Φ can be associated with $(-\underline{\mathbf{F}}^{\mathrm{T}}\dot{\mathbf{x}})$. In the same way, Ω corresponds to the energy momentum tensor $\underline{\mathbf{M}}$ and Π_B corresponds to the configurational force in volume $\mathbf{g}_B$.

In the consequence, Equation $(17)_2$ yields the configurational momentum balance on the phase boundary

$$\rho[\![\underline{\mathbf{F}}^{\mathrm{T}}\dot{\mathbf{x}}]\!]\mathrm{v_n} = [\![\underline{\mathbf{M}}]\!]\mathbf{n} + \mathbf{g}_S \quad \text{on S.} \tag{18}$$

Assuming that in Equation (11) the interface dissipation vanishes, i.e. $\omega_S = 0$, Equation (11) is the normal component of Equation (18). Thus we have established the identity

$$\tau_{\mathrm{n}} = -\mathbf{n}\cdot\mathbf{g}_S = \mathbf{n}\cdot[\![\underline{\mathbf{M}}]\!]\mathbf{n} - \rho\mathbf{n}\cdot[\![\underline{\mathbf{F}}^{\mathrm{T}}\dot{\mathbf{x}}]\!]\mathrm{v_n}. \tag{19}$$

2.2 Evolution Equations

Based on the calculated configurational forces as shown before, microstructural evolution can now be transferred into numerical models. In this context, appropriate evolution laws are defined.

At first, the local dissipation inequality (11) is integrated over the complete phase boundary

$$\mathscr{D} = \int_S \tau_{\mathrm{n}}\mathrm{v_n}\,\mathrm{dA} \geq 0. \tag{20}$$

Due to a geometrical restriction to two dimensional ellipsoids, Equation (20) can be rewritten according to parametrization of the shape of the ellipse

$$\begin{aligned}\mathrm{v_n} &= \dot{\boldsymbol{\mathscr{X}}}(\mathrm{m},\mathrm{V})\cdot\mathbf{n}\\ &= \left(\frac{\partial\boldsymbol{\mathscr{X}}}{\partial\mathrm{m}}\cdot\mathbf{n}\right)\dot{\mathrm{m}} + \left(\frac{\partial\boldsymbol{\mathscr{X}}}{\partial\mathrm{V}}\cdot\mathbf{n}\right)\dot{\mathrm{V}},\end{aligned} \tag{21}$$

see Mueller (2001) and Kolling (2001) for details. By means of vector $\boldsymbol{\mathscr{X}}$, the inclusion's configuration is defined. The quantities V and m denote volume and aspect ratio of the inclusion, where m=(a-b)/(a+b), with a and b as the semi-axes of the ellipsoid. With Equations (20) and (21), the global dissipation inequality yields

$$\begin{aligned}\mathscr{D} &= \int_S \tau_{\mathrm{n}}\left[\left(\frac{\partial\boldsymbol{\mathscr{X}}}{\partial\mathrm{m}}\cdot\mathbf{n}\right)\dot{\mathrm{m}} + \left(\frac{\partial\boldsymbol{\mathscr{X}}}{\partial\mathrm{V}}\cdot\mathbf{n}\right)\dot{\mathrm{V}}\right]\,\mathrm{dA}\\ &= \tau_{\mathrm{m}}\,\dot{\mathrm{m}} + \tau_{\mathrm{V}}\dot{\mathrm{V}} \geq 0.\end{aligned} \tag{22}$$

In Equation (22), the quantities τ_{V} and τ_{m} represent the consistent driving force with respect to the modification of volume and shape.

At the present stage, we neglect reorientation of the inclusion. This seems to be a reasonable assumption if the semi-axis agree with the principle loading directions.

To change the inclusion's configuration, relations $\dot{\mathrm{m}} = f(\tau_{\mathrm{m}})$ and $\dot{\mathrm{V}} = f(\tau_{\mathrm{V}})$ that fulfil the dissipation inequality (22) have to be chosen. In this context, the physical behaviour of voids has to be taken into account, e.g. void growth is suppressed for hydrostatic pressure. Though, an evolution in

shape is admissible. This means that the inclusion is able to change its shape in vertical direction during horizontal loading and vice versa.

In the case of simultaneous volume evolution, the rate of shape modification depends on the current volume additionally. To avoid this effect, we relate τ_{m} to the current inclusion's volume by

$$\dot{\mathrm{m}} = \alpha\ \tau_{\mathrm{m}} \frac{V_0}{V}, \tag{23}$$

with a material parameter $\alpha > 0$. In Equation (23), V_0 denotes the initial volume of the inclusion. Based on Equation (22), other relations can be created, too.

Due to (22), we also have to fulfil the constraint

$$\tau_{\mathrm{V}}\ \dot{\mathrm{V}} \geq 0, \tag{24}$$

when $\tau_{\mathrm{V}} \geq 0$. In consequence, we allow void growth in the case of a new exceeding amount of τ_{V} only. This approach coincides with the basic idea of evolution of the phenomenological damage variable d (Equations (1) and (2)). As a suitable relation we use

$$\mathrm{V} = \mathrm{V}(\beta) = \mathrm{V}_0 + (\mathrm{V}_{\max} - \mathrm{V}_0)(1 - \exp(\beta/\eta)). \tag{25}$$

The quantity η denotes a saturation parameter to control the rate of void growth. The remaining quantity

$$\beta = \beta(t) = \max_{s\in[0,t]} \tau_{\mathrm{V}}(s) \tag{26}$$

denotes the maximum driving force attained up to the current time t. Consequently, the inequality (22) is preserved.

According to Equation (26), τ_{V} depends on the boundary position. Thus, under constant loads self growth of voids can be expected. Hence, we modify the evolution law by relating τ_{V} to the current surface

$$\beta(t) = \max_{s\in[0,t]} \left[\tau_{\mathrm{V}}(s) \frac{A(0)}{A(s)} \right], \tag{27}$$

where $A(s) = \int_{S(s)} \mathrm{dA}$. Void growth at hydrostatic compression has to be avoided, too. Though configurational forces cannot distinguish between compression pressure or dilatation. In this context, we use the applied strains $\underline{\mathbf{E}}^{\infty}$ as additional constraints. With the aid of McCauley brackets defined by

$$\langle \mathrm{tr}\underline{\mathbf{E}}^{\infty} \rangle = 0.5(\mathrm{tr}\underline{\mathbf{E}}^{\infty}) + 0.5\,|(\mathrm{tr}\underline{\mathbf{E}}^{\infty})|, \tag{28}$$

we extend the evolution Equation (27) to give

$$\beta(t) = \max_{s\in[0,t]} \left[\tau_{\mathrm{V}}(s) \frac{A(0)}{A(s)} \frac{\langle \mathrm{tr}\underline{\mathbf{E}}^{\infty} \rangle}{\mathrm{tr}\underline{\mathbf{E}}^{\infty}} \right]. \tag{29}$$

2.3 Critical Void Volume

In the case of critical void volume, the assumed boundary conditions do not hold anymore. At a certain volume voids coalescence occur that can not be captured by the present model. This critical value is comparable to the upper bound of the damage variable d. To avoid further void growth beyond a critical threshold $\mathrm{V}_{\mathrm{crit}}$, we define an additional penalty term

$$\Pi_{\mathrm{pen}} = (0.5\mathrm{p}(\mathrm{V} - \mathrm{V}_{\mathrm{crit}}) + 0.5\mathrm{p}(|\mathrm{V} - \mathrm{V}_{\mathrm{crit}}|))^{\mathrm{m}}. \tag{30}$$

According to (30), the current volume V is penalized by an additional energy. Derivation of Equation (30) with respect to the volume leads to a reduction of the driving forces

$$\mathscr{D} = \tau_{\mathrm{m}}\ \dot{\mathrm{m}} + \left(\tau_{\mathrm{V}} - \frac{\partial \Pi_{\mathrm{pen}}}{\partial \mathrm{V}} \right) \dot{\mathrm{V}} \geq 0 \tag{31}$$

for the volume modification in the dissipation inequality (22). Consequently, further growth is avoided.

3 Homogenization

An important issue of two scale simulations is the transfer of field quantities between the scales. The macrostresses and macrostrains of the upper scale are related to the stresses and strains of the microscale. An important quantity which yields the information of the loading state is the deformation gradient $\underline{\mathbf{F}}$. Due to microstructural inhomogeneities, its microscopic average

$$\underline{\mathbf{F}}_{\mathrm{mac}} = \langle \underline{\mathbf{F}}_{\mathrm{mic}} \rangle = \langle \underline{\mathbf{F}} \rangle = \frac{1}{\mathrm{V}} \int_{B} \underline{\mathbf{F}}(\mathbf{X})\ \mathrm{dV} \tag{32a}$$

corresponds to the macroscopic value. Based on Gauss theorem, we can modify Equation (32a) to obtain

$$\langle \underline{\mathbf{F}} \rangle = \frac{1}{\mathrm{V}} \int_{\partial B} \mathbf{x} \otimes \mathbf{N} \, \mathrm{dA} = \underline{\mathbf{1}} + \frac{1}{\mathrm{V}} \int_{\partial B} \mathbf{u} \otimes \mathbf{N} \, \mathrm{dA}. \quad (32b)$$

With a constant displacement gradient $\underline{\mathscr{H}} = const.$ and $\mathbf{u}|_{\partial B} = \underline{\mathscr{H}} \cdot \mathbf{X}$, relation $(32b)_2$ can be reformulated to

$$\langle \underline{\mathbf{F}} \rangle = \underline{\mathbf{1}} + \frac{1}{\mathrm{V}} \int_{\partial B} (\underline{\mathscr{H}} \cdot \mathbf{X}) \otimes \mathbf{N} \, \mathrm{dA} = \underline{\mathbf{1}} + \underline{\mathscr{H}} = \underline{\mathscr{F}}, \quad (32c)$$

see Loehnert (2004).

To homogenize the stress in a similar way, we are restricted to a stress quantity which is defined in the reference configuration. Analogous to Equation (32a), the transposed of First Piola Kirchhoff stress of the macroscale

$$\underline{\mathbf{P}}^{\mathrm{T}}_{\mathrm{mac}} = \langle \underline{\mathbf{P}}^{\mathrm{T}}_{\mathrm{mac}} \rangle = \left\langle \underline{\mathbf{P}}^{\mathrm{T}} \right\rangle = \frac{1}{\mathrm{V}} \int_{B} \underline{\mathbf{P}}^{\mathrm{T}}(\mathbf{X}) \, \mathrm{dV} \quad (33a)$$

can be computed by averaging of its microscale value. Based on the momentum balance (Equation (4), body forces are neglected), we can use the identity $\mathrm{Div}(\mathbf{X} \otimes \underline{\mathbf{P}}) = \underline{\mathbf{P}}^{\mathrm{T}} - \mathbf{X} \otimes \rho \ddot{\mathbf{x}}$ as well as the Gauss theorem again, to modify Equation (33a) to

$$\left\langle \underline{\mathbf{P}}^{\mathrm{T}} \right\rangle = \frac{1}{\mathrm{V}} \int_{\partial B} \mathbf{X} \otimes \underline{\mathscr{P}} \cdot \mathbf{N} \, \mathrm{dA} + \frac{1}{\mathrm{V}} \int_{B} \mathbf{X} \otimes \rho \ddot{\mathbf{x}} \, \mathrm{dV}, \quad (33b)$$

where $\underline{\mathscr{P}} = const.$ is defined as the First Piola Kirchhoff stress on the boundary in case of a boundary traction $\mathbf{T}|_{\partial B} = \underline{\mathscr{P}} \cdot \mathbf{N}$. With $\mathrm{Div}(\mathbf{X} \otimes \underline{\mathscr{P}}) = \underline{\mathscr{P}}^{\mathrm{T}} - \mathbf{X} \otimes \rho \ddot{\mathbf{x}}$, we get finally the correlation

$$\left\langle \underline{\mathbf{P}}^{\mathrm{T}} \right\rangle = \underline{\mathscr{P}}^{\mathrm{T}} + \frac{1}{\mathrm{V}} \int_{B} \mathbf{X} \otimes \rho \ddot{\mathbf{x}} \, \mathrm{dV}. \quad (33c)$$

Usually, the Cauchy stress is required. In that case, we use the mean value of First Piola Kirchhoff stress according to Equation (33c) and the relation

$$\langle \underline{\boldsymbol{\sigma}} \rangle = \left(\det \langle \underline{\mathbf{F}} \rangle\right)^{-1} \langle \underline{\mathbf{F}} \rangle \left\langle \underline{\mathbf{P}}^{\mathrm{T}} \right\rangle, \quad (34)$$

see Nemat-Nasser (1999). Thus, after numerical investigation of the microscale, the mean Cauchy stress can be transferred to the macroscale.

4 Numerical Implementation in FEM

In order to calculate the driving force on the inclusions, we apply the weak formulation of the configurational momentum balance according to Equation (15). Due to the finite element discretization of the structure, the balance equation in volume B has to be used.

After multiplying with a test function η and integration over the volume, we get

$$\int_{B} \left(\rho \, (\dot{\overline{\underline{\mathbf{F}}^{\mathrm{T}} \dot{\mathbf{x}}}}) + \mathrm{Div} \, \underline{\mathbf{M}} + \mathbf{g} \right) \cdot \eta \; dV = 0. \quad (35)$$

With $(\mathrm{Div}\underline{\mathbf{M}}) \cdot \eta = \mathrm{Div}\,(\underline{\mathbf{M}} \cdot \eta) - \underline{\mathbf{M}} : \nabla_{\mathbf{X}} \eta$ and the Gauss theorem $\int_B \mathrm{Div}\,(\underline{\mathbf{M}} \cdot \eta) \; dV = \int_{\partial B} \underline{\mathbf{M}}\, \mathbf{n} \cdot \eta \; dA$, Equation (35) can be rearranged to give

$$\int_{B} \left[\rho \, (\dot{\overline{\underline{\mathbf{F}}^{\mathrm{T}} \dot{\mathbf{x}}}}) \cdot \eta - \underline{\mathbf{M}} : \nabla_{\mathbf{X}} \eta + \mathbf{g} \cdot \eta \right] dV = 0 \, , \quad (36)$$

where we took into account that the test function η vanishes on the boundary ∂B. Henceforth, with an approximation of the test function in each finite element Ω by nodal values η^l and shape functions N^l we get the discrete configurational force

$$\mathbf{G}^{\,l} = \bigcup_{e=1}^{n_e} \int_{\Omega} \left\{ \underline{\mathbf{M}} \nabla_{\mathbf{X}} N^{\,l} - \rho \, (\dot{\overline{\underline{\mathbf{F}}^{\mathrm{T}} \dot{\mathbf{x}}}}) \, N^{\,l} \right\} d\Omega, \quad (37)$$

where the operator $\bigcup$ denotes the assembling of all adjacent elements of the node l. The discrete driving force on a phase boundary can be computed according to Equation $(19)_1$ by multiplying with the normal vector on the phase boundary

$$\mathscr{T}^{\,l}_{n} = -\mathbf{n} \cdot \mathbf{G}^{\,l}. \quad (38)$$

5 Small Strains

In the case of small strains, a few simplifications can be made. At first, the difference between reference and current configuration vanishes ($\mathbf{X} \rightarrow \mathbf{x}$, $\underline{\mathbf{P}} \rightarrow \underline{\boldsymbol{\sigma}}$). The deformation state can now be described by the displacement gradient $\underline{\mathbf{H}} = \nabla_{\mathbf{x}} \mathbf{u}$ and $\underline{\boldsymbol{\varepsilon}} = 0.5(\underline{\mathbf{H}} + \underline{\mathbf{H}}^{\mathrm{T}})$.

Furthermore, the dissipation inequality (11) on the phase boundary is modified to give

$$(\mathbf{n} \cdot [\![\underline{\mathbf{C}}]\!] \mathbf{n} - \mathrm{v_n} \rho \mathbf{n} \cdot [\![\, (\nabla_{\mathbf{x}} \mathbf{u})^{\mathrm{T}} \dot{\mathbf{x}}]\!] = \omega_S \Theta \geq 0, \quad (39)$$

where in analogy to Equation (40) the quantity

$$\underline{\mathbf{C}} = \left(\psi - \frac{1}{2}\rho \left|\dot{\mathbf{x}}\right|^2 \right) \underline{\mathbf{1}} - (\nabla_{\mathbf{x}} \mathbf{u})^{\mathrm{T}} \underline{\boldsymbol{\sigma}} \tag{40}$$

denotes the energy momentum tensor for small strains, with

$$\psi(\underline{\boldsymbol{\varepsilon}}, \mathbf{x}) = \begin{cases} \frac{1}{2}\, \underline{\boldsymbol{\varepsilon}}(\mathbf{x}) : \mathbb{C}^- \, \underline{\boldsymbol{\varepsilon}}(\mathbf{x}) & \forall\, \mathbf{x} \in B^- \\ \frac{1}{2}\, \underline{\boldsymbol{\varepsilon}}(\mathbf{x}) : \mathbb{C}^+ \, \underline{\boldsymbol{\varepsilon}}(\mathbf{x}) & \forall\, \mathbf{x} \in B^+ \end{cases}. \tag{41}$$

In Equation (41), the potential depends on the stiffness tensor $\mathbb{C}^{+/-}$.

A very usefull simplification in small strains consists in an analytical solution of the driving force in Equation (11), which is given by

$$\tau_{\mathrm{n}} = -\frac{1}{2} [\![\mathbb{C}]\!]\, \underline{\boldsymbol{\varepsilon}}^- \cdot \underline{\Omega}^{-1}(\mathbf{n}) [\![\mathbb{C}]\!] \underline{\boldsymbol{\varepsilon}}^- + \frac{1}{2} \underline{\boldsymbol{\varepsilon}}^- : [\![\mathbb{C}]\!] \underline{\boldsymbol{\varepsilon}}^-, \tag{42}$$

where $\Omega_{\mathrm{ik}}(\mathbf{n}) = \mathbb{C}^+_{\mathrm{ijkl}} \mathrm{n_j n_l}$ denotes the acoustic tensor and $[\![\mathbb{C}]\!] = \mathbb{C}^+ - \mathbb{C}^-$ defines the jump in the stiffness, see Schmidt (1997). The quantity $\underline{\boldsymbol{\varepsilon}}^-$ denotes the strain in the inclusions. These strains are computed analytically due to the ellipsoidal shape by the method of equivalent eigenstrain. Within this context, the inclusion's stiffness $\mathbb{C}^-$ is transferred to an equivalent model where $\mathbb{C}^-$ is substituted by an arbitrary chosen stiffness $\mathbb{C}^{\mathrm{c}}$. Then, the induced differences in stresses are corrected by an equivalent eigenstrain $\underline{\varepsilon}^*$

$$\begin{aligned} \underline{\boldsymbol{\sigma}}^{-'} &= \underline{\boldsymbol{\sigma}}^- - \underline{\boldsymbol{\sigma}}^{\mathrm{c}} \\ &= \mathbb{C}^- \, \underline{\boldsymbol{\varepsilon}}^- - \mathbb{C}^{\mathrm{c}} (\overbrace{\underline{\boldsymbol{\varepsilon}}^{\mathrm{c}}}^{\underline{\boldsymbol{\varepsilon}}^-} - \underline{\boldsymbol{\varepsilon}}^{-'}) \\ &= \mathbb{C}^{\mathrm{c}} [\, \underline{\boldsymbol{\varepsilon}}^{-'} + \underbrace{(\mathbb{C}^{\mathrm{c}})^{-1} (\mathbb{C}^- - \mathbb{C}^{\mathrm{c}}) (\underline{\boldsymbol{\varepsilon}}^{-'} + \underline{\boldsymbol{\varepsilon}}^{\mathrm{c}})}_{-\underline{\boldsymbol{\varepsilon}}^*}]. \end{aligned} \tag{43}$$

$\underline{\boldsymbol{\varepsilon}}^{\mathrm{c}}$ denotes the macroscopic strain that corresponds to external strains at the microscale. The equivalent eigenstrain $\underline{\boldsymbol{\varepsilon}}^*$ induces a modification of the inclusion's total strain. In this context, a further important solution of Eshelby (1957), known as Eshelby-tensor, is used.

Based on this Eshelby-tensor $\mathbb{S}$ (see also Mura (1991)), the inclusion's total strains due to arbitrary eigenstrains can be calculated.

The deviation in stress of Equation (43) is obtained using the approach ($\underline{\boldsymbol{\varepsilon}}^{-'} = \mathbb{S} : \underline{\boldsymbol{\varepsilon}}^*$). The fourth-order tensor $\mathbb{S} = \mathbb{S}(\nu, \mathrm{m})$ depends on Poisson's ratio and the shape of the ellipse. In the case of the assumption that the chosen continuous stiffness coincides to those of the matrix material ($\mathbb{C}^{\mathrm{c}} = \mathbb{C}^+$), the equivalent stiffness of an embedded ellipsoid yields

$$\underline{\boldsymbol{\varepsilon}}^* = -[\mathbb{S} + (\mathbb{C}^- - \mathbb{C}^+)^{-1} : \mathbb{C}^+]^{-1} : \underline{\boldsymbol{\varepsilon}}^{\mathrm{c}}. \tag{44}$$

The inclusions's strain $\underline{\boldsymbol{\varepsilon}}^-$ may be computed as

$$\underline{\boldsymbol{\varepsilon}}^- = \underbrace{\left[\mathbb{I} + \mathbb{S} : (\mathbb{C}^+)^{-1} : (\mathbb{C}^- - \mathbb{C}^+)\right]^{-1}}_{\mathbb{A}^\infty} : \underline{\boldsymbol{\varepsilon}}^{\mathrm{c}}. \tag{45}$$

Based on the fourth order influence tensor $\mathbb{A}^\infty$, a relation between external strains and the true strains in the inclusion is available. For homogeneous stiffness of the involved phases, the influence tensor coincides with the unit tensor $\mathbb{I}$.

In order to transfer the global information into this micromodel according to the Equations (33b) and (33c), both scales are coupled as follow:

$$\underline{\boldsymbol{\varepsilon}}_{\mathrm{mac}} = \langle \underline{\boldsymbol{\varepsilon}}_{\mathrm{mic}} \rangle = \frac{1}{\mathrm{V}} \int_{\mathrm{B}} \underline{\boldsymbol{\varepsilon}}(\mathbf{x}) \, \mathrm{dV}, \tag{46a}$$

$$\langle \underline{\boldsymbol{\sigma}}_{\mathrm{mic}} \rangle = \frac{1}{\mathrm{V}} \int_{\mathrm{B}} \underline{\boldsymbol{\sigma}}(\mathbf{x}) \, \mathrm{dV} = \underline{\boldsymbol{\sigma}}_{\mathrm{mac}} + \int_{\mathrm{B}} \mathbf{x} \otimes \rho \ddot{\mathbf{x}} \, \mathrm{dV}, \tag{46b}$$

(see Gross and Seelig (2001)). Consequently, a relation between mean values of the stress and strain fields can be given by

$$\langle \underline{\boldsymbol{\sigma}} \rangle = \mathbb{C}^* : \langle \underline{\boldsymbol{\varepsilon}} \rangle. \tag{47}$$

According to Equation (47), the essential quantity, that has to be found, is the effective stiffness tensor $\mathbb{C}^*$. Using Equation (45) and a linear interpolation of the phase fractions yields

$$\mathbb{C}^* = \left[(\mathbb{C}^+)^{-1} + \frac{\mathrm{V}^-}{\mathrm{V}} \left((\mathbb{C}^-)^{-1} - (\mathbb{C}^+)^{-1} \right) \mathbb{A}^\infty \right]^{-1}.$$

(48)

A detailed discussion of relations between the quantities of the macro- and microscale is given by Mura (1991).

Based on Equation (48), the importance of microstructural evolution on the macroscale is evident. On the one hand, increasing the volume reduces the global stiffness. However, this conclusion holds only if $\mathbb{C}^- < \mathbb{C}^+$. On the other hand, the change of the inclusion's shape results in a change of the stiffness. The influence tensor increases and the global stiffness decreases.

6 Examples

The suggested modeling technique is illustrated by two examples where structures at both small and finite strains are discussed. To simplify matters, we restrict our attention to the microscale. Though, the interaction between micro- and macroscale will be pointed out clearly. The present methodology can be applied to two scale simulations. For further applications see Mueller and Gross (2001) and Timmel, Kaliske and Kolling (2005).

6.1 Evolution at small strains

At first, we consider a system with prescribed displacements as depicted on the left hand side of Figure 3. Let us suppose a linear elastic behaviour

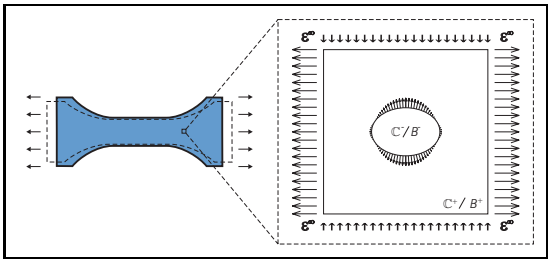

Figure 3: global structure and representative micro model

of the material. To approximate this structural behaviour numerically, a constitutive model according to Equation (48) is chosen.
To approach additionally the damage effects based on the phenomenological model (Equations (1) and (2)), the stress softening is taken into account by $\underline{\boldsymbol{\sigma}} = (1-\mathrm{d})\mathbb{C} : \underline{\boldsymbol{\varepsilon}}$. Here, the global reduction of stiffness tensor $\mathbb{C}$ leads to the reduction of the stress.

Using the methodology of two scale investigations, this reduction of the tangent stiffness will be substituted by the microstructural evolution model. Thereby, we define a representative microsystem as shown on the right hand side of Figure 3. This system consists of a unit cell with volume V_B, which contains a soft inclusion ($\mathbb{C}^- = (1/10)\,\mathbb{C}^+$) with an initial volume $V_{B^-} = (1/50)V_{B^+}$.
The microstructure is subjected to a horizontal displacement of the left boundary and boundary conditions are used else. The displacement is increased linearly up to maximum deformation before unloading is applied, i.e. the time-deformation path is triangular shaped. The evolution parameters are chosen for the model problem.

6.1.1 Algorithmic Procedure and Results

The presented material model based on a microstructural evolution approach has been implemented into an explicit finite element program. At first, we describe the implementation into the context of the algorithmic sequence of the code.
At the beginning, the interface of the finite element code transfers the strains $\underline{\boldsymbol{\varepsilon}}$ of the macroscale, which correspond according to Equation (46a) to the far-field strains $\underline{\boldsymbol{\varepsilon}}^{\mathrm{c}}$ of the microscale, see Equation (45). The same initial configuration of the microstructure is used in each Gauss point. To modify these configurations, we use the driving forces according to Equation (42) as described before.

The main advantage consists of the purely analytical solution of the two scale procedure. Based on the right hand side of Figure 3, the external load and the driving forces acting on the microstructure are shown. The driving forces acting on the inclusion's interface represent again the direction of energy reduction in the case of the applied load.

Based on the evolution law (22), the configura-

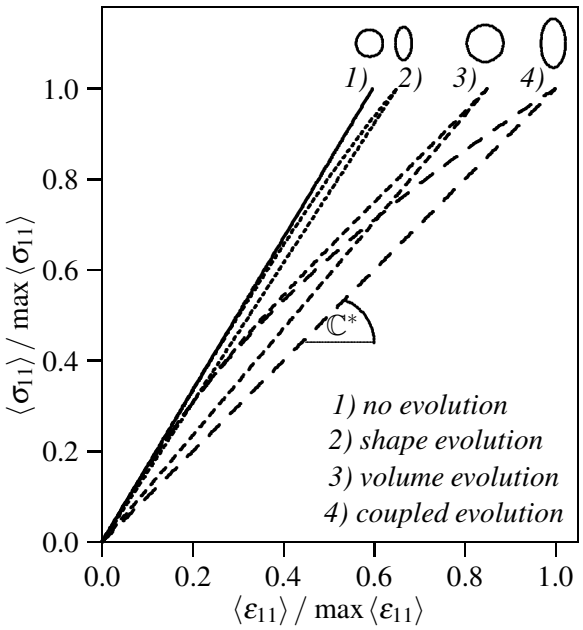

Figure 4: stress softening at different microstructural evolutions

tion of the inclusion is computed for the next iteration step. Finally, we determine the effective stiffness according to Equation (48). As shown in Figure 4, a number of stress-strain relations are pointed out to show the effects of the microstructural evolution on the macroscale. In the case of path *1)*, where all kinds of evolutions are suppressed, loading and unloading curves are identical. At paths *2)* and *3)*, an uncoupled evolution in shape and volume is pointed out.
In the case of a coupled evolution at path *4)*, the stress softening is clearly seen. The related configuration of the inclusion can be considered close to the realistic configurations of voids in real structures. During unloading, the evolution of microstructures is kept constant.

6.2 Evolution at finite strains

In the next step, the two scale method is used to analyze the damage behaviour of rubberlike materials, i.e. for large deformation.

In this context, the microstructure is constituted by Yeoh model, see Yeoh (1990) for details, where the material parameters are $C_1^- = (1/10)C_1^+$, $C_2^- = (1/100)C_2^+$ and $C_3^{-/+} = 0$.

In contrast to the small strain limit as shown before, methods to compute configurational forces analytically for finite strains do not exist. For arbitrary finite strains, the description of the microstructural evolution is based on a separate numerical treatment.

Based on Equations (37) and (38), the driving forces on the ellipsoidal modification are computed numerically in a postprocessing step.

Due to separate numerical investigations on both scales, however, the computation time increases strongly. For the two scale approach in the case of finite strains, the external load is applied by the deformation gradient.

6.2.1 Algorithmic Procedure and Results

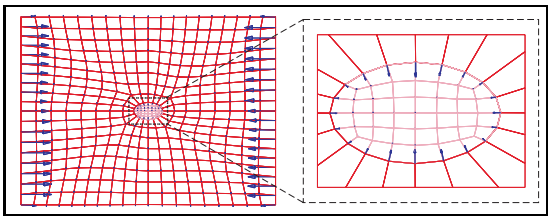

Figure 5: configurational forces on microstructure

Based on Equations (37) and (38), the driving forces are computed at the end of each time step. Figure 5 shows the configurational forces acting on the boundary and on the interface between inclusion and surrounding material. Due to same loading conditions, the configurational forces on the interface are qualitatively similar to the previous example.

Like in the first example, the modified geometry of the inclusion will be computed at the end of the time step t_n.

Furthermore, we calculate the average strain field. The strain can be considered as macroscopic strain in the Gauss point.

In the follow time step, a modified reference configuration is needed. Hence, the simulation is interrupted at this point.

In a next step, based on stored informations of the modified inclusion, the input file is changed and a new simulation is started that is interrupted at the

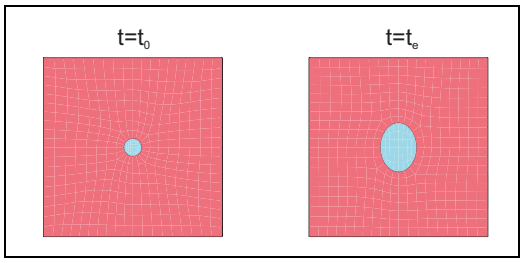

Figure 6: configuration before and after loading

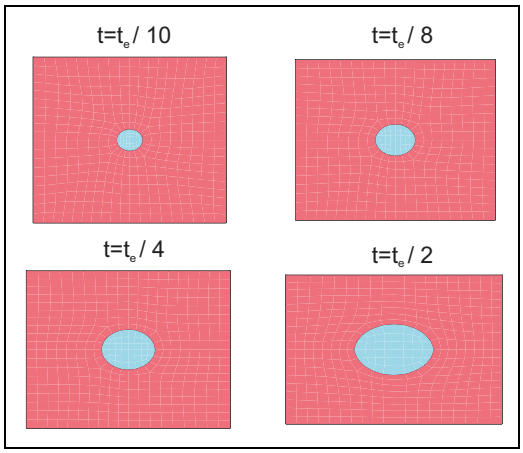

Figure 7: evolution at different deformations

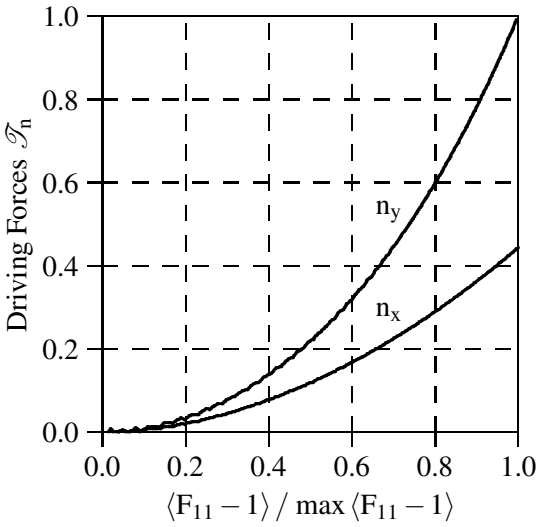

Figure 8: main driving forces on inclusion

time step t_{n+1}. These procedure is repeated over and over. Based on this numerical procedure, a stepwise change of the microstructure is achieved. Thus, the softening behaviour of rubberlike materials can be taken into account.

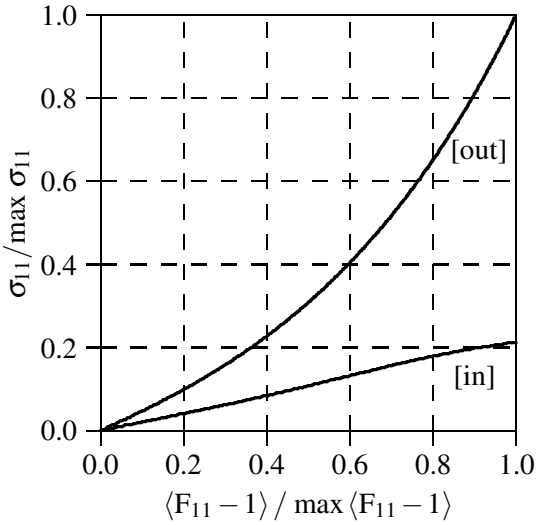

Figure 9: microstructure's stress

On the left hand side of Figure 6, the initial configuration of an arbitrary chosen microstructure, which represents the material behaviour in the integration point, is shown. In the framework of a benchmark study, the shown microstructure will be subjected to prescribed deformations as given in the previous example.

In this example, however, we have chosen an increased amplitude of the time-deformation path. Generally, these deformations are given by the macro scale in two scale finite element methods.

However, such kind of interaction is neglected in this example. In Figure 7, the qualitative results of the numerical simulation are shown. The evolution of the volume during different deformation steps is depicted. Due to finite strains, the ellipsoidal characteristic is shown on the right hand side of Figure 6. In Figure 8, horizontal as well as vertical driving forces acting on inclusion are depicted. Here, the initial configuration without evolution is analyzed. Based on this different driving forces, an ellipsoidal inclusion shape can be proven. Based on Figure 9, the stress-deformation paths from matrix and inclusion are illustrated.

In particular, the nonlinear material behaviour is pointed out in Figures 8 and 9. Finally, the stress softening on the macroscale is illustrated in Figure 10. The damage behaviour is shown by com-

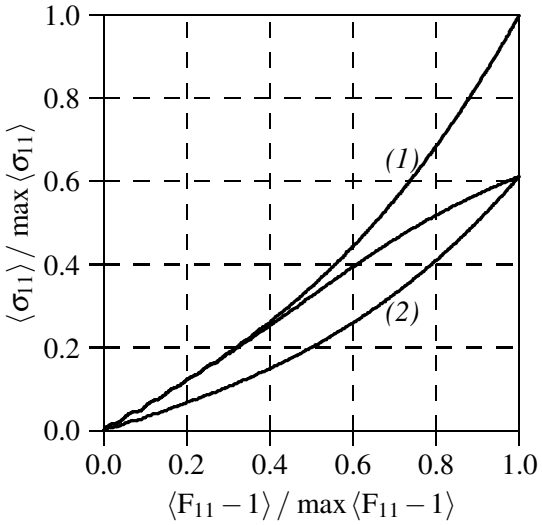

Figure 10: mean stress at loading/unloading for (*1*)continuous/(*2*)evolving inclusion

parison of the evolved paths with and without microstructural evolution. Due to the chosen linear relation of the evolution between driving forces and inclusion's geometrical change, softening occurs primarily at large strains. In particular, this behaviour can be modified by exponential relations.

Further applications in the field of micromechanics can be found in Gao, Zheng and Yao (2006) and Zhang and Xia (2005).

7 Conclusions and Outlook

In the present paper, we introduced a new approach to take softening behaviour of hyperelastic materials into account using a two scale method. In this context, a defined microsystem, where soft inclusions are embedded in stiffer matrix material, is investigated numerically.

The description of the damage behaviour of rubber-like materials by the concept of configurational forces on the microscale is one of the central ideas of this investigation. Due to the evolution at microscale, the overall structural behaviour can be modified. Apart from the theoretical basics the implemenation into an explicit finite element program is shown and the methodology is applied to some illustrative examples.

The generalization of the present model to anisotropic material behaviour and its application to complex structures are topics of further investigations.

References

Coleman, B. D.; Noll, W. (1963): The Thermodynamics of Elastic Materials with Heat Conduction and Viscosity. *Archive for Rational Mechanics and Analysis*, vol. 13, pp. 167–178.

Eshelby, J. D. (1957): The determination of the elastic field of an ellipsoidal inclusion and related problems. *Proceedings of the Royal Society London*, vol. 241, pp. 376–396.

Eshelby, J. D. (1970): Energy relations and the energy-momentum tensor in continuum mechanics. *In Kanninen M.F.: Inelastic behaviour of solids, Mc Graw Hill, New York*, pp. 87–112.

Gao, L.; Zheng, X.; Yao, Z. (2006): Numerical Simulation of Elastic Behaviour and Failure Processes in Heterogeneous Material. *CMC: Computers, Materials, and Continua*, vol. 3, pp. 25–36.

Gross, D.; Seelig, T. (2001): *Bruchmechanik mit einer Einführung in die Mikromechanik*. Springer, Berlin.

Kolling, S. (2001): *Zur numerischen Simulation von Morphologieänderungen in mikroheterogenen Materialien*. Institut für Mechanik, TU Darmstadt, Darmstadt.

Lemaitre, J.; Desmorat, R. (2005): *Engineering Damage Mechanics*. Springer, Berlin.

Loehnert, S. (2004): *Computational Homogenization of Microheterogeneous Materials at Finite Strains Including Damage*. Institut für Baumechanik und numerische Mechanik, Universität Hannover, Hannover.

Maugin, G. A. (1993): *Material Inhomogeneities in Elasticity*. Chapman and Hall, London.

Mueller, R. (2001): *3D-Simulation der Mikrostrukturentwicklung in Zwei-Phasen-Materialien*. Institut für Mechanik, TU Darmstadt, Darmstadt.

Mueller, R.; Gross, D. (2001): A time dependent constitutive law for materials with microstructural evolution. *Mechanics of Materials*, vol. 22, pp. 63–76.

Mura, T. (1991): *Micromechanics of Defects in Solids*. Kluwer, London.

Nemat-Nasser, S. (1999): Averaging theorems in finite deformations plasticity. *Mechanics of Materials*, vol. 22, pp. 493–523.

Schmidt, I. (1997): *Gleichgewichtsmorphologien elastischer Einschlüsse*. Institut für Mechanik, TU Darmstadt, Darmstadt.

Timmel, M.; Kaliske, M.; Kolling, S. (2004): On the modeling of rubber-like materials subjected to dynamic loading. *Proceedings of the 3rd LS-DYNA Forum, Bamberg, Germany*.

Timmel, M.; Kaliske, M.; Kolling, S. (2005): A new evaluation criterion for damaged structures. *Proceedings of the 4th LS-DYNA Forum, Bamberg, Germany*.

Yeoh, O. H. (1990): Characterization of Elastic Properties of Carbon-Black-Filled Rubber Vulcanizates. *Rubber Chemistry and Technology*, vol. 63, pp. 792–805.

Zhang, Y.; Xia, Z. (2005): Micromechanical Analysis of Interphase Damage for Fiber Reinforced Composite Laminates. *CMC: Computers, Materials, and Continua*, vol. 2, pp. 213–226.